Paramagnetic Spectra of Substituted Sapphires—Part I: Ruby*

By E. O. SCHULZ-DU BOIS

(Manuscript received September 29, 1958)

The paramagnetic resonance properties of Cr^{+++} ions in Al_2O_3 (ruby) were investigated theoretically and experimentally in order to obtain information necessary for the application of this material as active material in a three-level solid-state maser (3LSSM). Numerically computed energy levels, together with their associated eigenvectors, are presented as a function of applied magnetic field for various orientations of the magnetic field with respect to the crystalline symmetry axis. A more detailed discussion is devoted to energy levels, eigenvectors and transition probabilities at angles 0°, 54.74° and 90°, where certain simple relations and symmetries hold. Paramagnetic spectra for signal frequencies between 5 and 24 kmc are shown; agreement between computed and measured resonance fields is satisfactory.

1. INTRODUCTION

Among the paramagnetic salts that have been used as active materials in three-level solid-state masers (3LSSM),[1, 2, 3] ruby shows rather desirable properties. While maser action of this material has been achieved at microwave signal frequencies of 3 to 10 kmc,[4] it should be possible to cover more than the whole centimeter microwave range. Perhaps even more important from a practical point of view are the bulk physical properties. Extremely good heat conductivity at low temperatures allows handling of relatively high microwave power dissipation. Industrial growth of large single crystals by the flame fusion technique and machinability with diamond tools make it possible to fabricate long sections of ruby to very close tolerances, a necessity in travelling-wave maser (TWM) development. Also, ruby can be bonded to metals, thus allowing a high degree of versatility in maser structural design. While the use of ruby in 3LSSM, in particular in nonreciprocal TWM, will be described

* This work is partially supported by the Signal Corps under Contract Number DA-36-039 sc-73224.

in forthcoming papers by members of Bell Telephone Laboratories, this paper is intended to give some background on paramagnetic resonance behavior of ruby.

In general, the paramagnetic resonance properties of an ion in a crystal can be completely described by a spin Hamiltonian containing a relatively small number of constants. In the case of ruby, these include the spectroscopic splitting factors parallel and perpendicular to the crystalline axis, $g_{\parallel}$ and $g_{\perp}$, the total spin $S = 3/2$ and the sign and magnitude of $2D$, the zero field splitting. Nuclear interactions can be neglected since the most abundant isotope, Cr^{52}, is nonmagnetic ($I = 0$) whereas the magnetic isotope, Cr^{53}, ($I = 3/2$) has small abundance (9.5 per cent) and leads to negligible line broadening only. Taking this into account, one can even predict on the basis of the total spin and the crystalline symmetry surrounding the Cr^{+++} ion that no other terms can occur in the spin Hamiltonian.

However, in order to predict operating conditions of this or other materials in a 3LSSM, it is necessary to know the separation of energy levels for supplying the proper pump and signal frequencies, the order of magnitude of the associated transition probabilities and perhaps other circumstances, such as coincidence of transition frequencies, which, by spin-spin interaction, may lead to shortening of the associated relaxation times (self-doping condition). In this paper, this information is evaluated by the formalism of the spin Hamiltonian and, at least in part, compared with experiment. The data presented graphically are intended to form an "atlas" of the ruby paramagnetic resonance properties. In the paper which follows, some general viewpoints are presented on modes in which paramagnetic materials can be operated as active materials in a 3LSSM. In further papers, paramagnetic spectra of other substitutional ions such as Co^{++} and Fe^{+++} in sapphire will be presented in order to furnish sufficient information to find coincidences of transition frequencies of Cr^{+++} with Co^{++} or Fe^{+++} lines resulting in reduced relaxation times (impurity-doping condition).

For a derivation of the method of spin Hamiltonians, reference should be made to such review articles as those by Bleaney and Stevens[5] and Bowers and Owen.[6] Knowledge of the associated formalism is perhaps desirable but not necessary for utilization of the results reported in this paper. Briefly, the spin Hamiltonian describes the energy of a paramagnetic ion arising from interaction with host crystal environment and applied magnetic field. Obeying quantum laws, the ion can exist in one of several states associated with discrete energy levels. Transitions between such states can occur if the energy balance ΔE is supplied to or

extracted from the ion. Given some probability for radiative transitions, these can be induced by applying a magnetic field of radio frequency $\nu = \Delta E/h$ (h = Planck's constant). If there are more transitions to the higher state, net absorption will be observed such as is normally observed with a spectrometer. If there are more transitions to the lower state, stimulated emission of energy will be observed such as is utilized for amplification in a 3LSSM.

II. THE SPIN HAMILTONIAN

The spin Hamiltonian of Cr^{+++} in Al_2O_3 was first published by Manenkov and Prokhorov[7], and later by Geusic[8] and Zaripov and Shamonin.[9] It was given in the form

$$\mathfrak{H} = g_\parallel H_z S_z + g_\perp (H_x S_x + H_y S_y) + D[S_z^2 - \tfrac{1}{3}S(S+1)]. \qquad (1)$$

The effective spin $S = 3/2$ is identical with the true spin. All Cr^{+++} ions in the crystal lattice show identical paramagnetic behavior, with the magnetic z-axis being the same as the trigonal symmetry axis of the crystal. The best values for the constants seem to be

$$2D = -2D' = -0.3831 \pm 0.0002 \text{ cm}^{-1} = -11.493 \pm 0.006 \text{ kmc},$$

$$g_\parallel = 1.9840 \pm 0.0006,$$

$$g_\perp = 1.9867 \pm 0.0006.$$

While it is customary in spectroscopy to express energy in units of cm^{-1} omitting a factor hc (h = Planck's constant, c = velocity of light), units of kmc are used simultaneously, omitting a factor of 10^9 h, because this allows direct interpretation in observed spectra.

In particular, the negative sign of D was obtained by Geusic.[8] He deduced this from the fact that $g_\parallel < g_\perp$, since in less than half-filled d-shell ions, such as Cr^{+++}, the spin-orbit coupling term λ is positive, and D is given by $2D = \lambda(g_\parallel - g_\perp)$. Sign and magnitude of D are in agreement with results of low-temperature static susceptibility measurements by Bruger.[10] In this work also, the negative sign of D was confirmed by comparing the relative intensities of two lines at liquid nitrogen and helium temperatures.

The spin Hamiltonian (1) can more conveniently be written in spherical coordinates:

$$\mathfrak{H} = g_\parallel H \cos\theta S_z + \tfrac{1}{2} g_\perp H \sin\theta (e^{-i\varphi} S_+ + e^{i\varphi} S_-) - D'[S_z^2 - \tfrac{1}{3}S(S+1)]. \qquad (2)$$

Here $S_\pm = S_x \pm iS_y$. In both representations (1) and (2) the crystalline axis was chosen to be the z-axis. While the choice of reference system is immaterial to obtaining eigenvalues (energy levels), this choice shows up in the associated eigenvectors. The eigenvectors have no direct physical interpretation; they must be evaluated in order to obtain transition probabilities. The transition probabilities most naturally obtained from eigenvectors of the Hamiltonian (2) are those which correspond to excitation by RF magnetic fields whose polarization is either linear and parallel to, or circular and perpendicular to, the *crystalline axis*.

In 3LSSM design, however, it seems more appropriate to analyze the performance in terms of RF magnetic fields whose polarization is either linear and parallel to, or circular and perpendicular to, the *applied field*. The corresponding eigenvectors and transition probabilities can, of course, be obtained from those belonging to the Hamiltonian (2) by a 4-by-4 transformation matrix. But it is more efficient to obtain them directly through a transformation of the original spin Hamiltonian (1) or (2) into a coordinate system with the z-axis parallel to the applied field. The result of this transformation is

$$\begin{aligned}\mathcal{H} = {} & (g_\parallel \cos^2\theta + g_\perp \sin^2\theta)\beta H S_z \\ & - D'(\cos^2\theta - \tfrac{1}{2}\sin^2\theta)[S_z^2 - \tfrac{1}{3}S(S+1)] \\ & - D'\tfrac{1}{2}\cos\theta\sin\theta[e^{-i\varphi}(S_zS_+ + S_+S_z) + e^{i\varphi}(S_zS_- + S_-S_z)] \\ & - D'\tfrac{1}{4}\sin^2\theta(e^{-2i\varphi}S_+^2 + e^{2i\varphi}S_-^2).\end{aligned} \tag{3}$$

III. ENERGY LEVELS AND EIGENVECTORS

From the Hamiltonian $\mathcal{H}$ (3), its energy eigenvalues W are found numerically by solving the fourth-order secular equation

$$\begin{gathered}\| \langle n \mid \mathcal{H} - W \mid m \rangle \| = 0, \\ n, m = 3/2,\ 1/2,\ -1/2,\ -3/2.\end{gathered} \tag{4}$$

The eigenvalues W are functions of H and θ, but not of φ since, because of the symmetry of the Hamiltonian, rotation about the z-axis does not change the physical situation. On the following plots (left-hand sections of Figs. 1 through 11) diagrams of energy levels W (in units of kmc) are shown as a function of applied field H (in units of kilogauss). Plots are given for angles θ from 0° to 90° in steps of 10° and, in addition, for 54.74°.

Also, by change of scales, dimensionless eigenvalues $y = W/D'$ are shown as functions of the dimensionless quantity $x = G/D'$, where

$$G = (g_\parallel \cos^2\theta + g_\perp \sin^2\theta)\beta H.$$

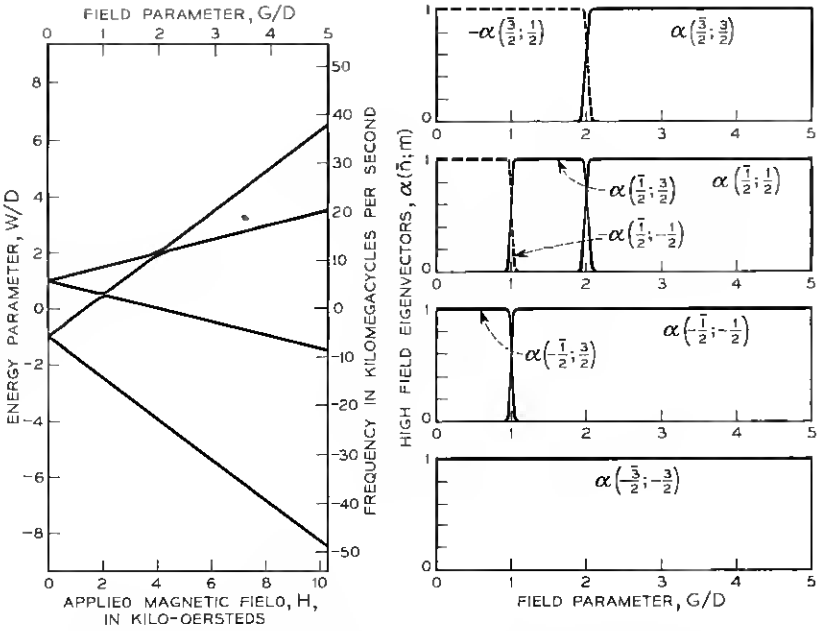

Fig. 1 — Energy levels and eigenvectors of the Cr^{+++} paramagnetic ion in ruby at angle $\theta = 0°$ between crystalline symmetry axis and applied magnetic field.

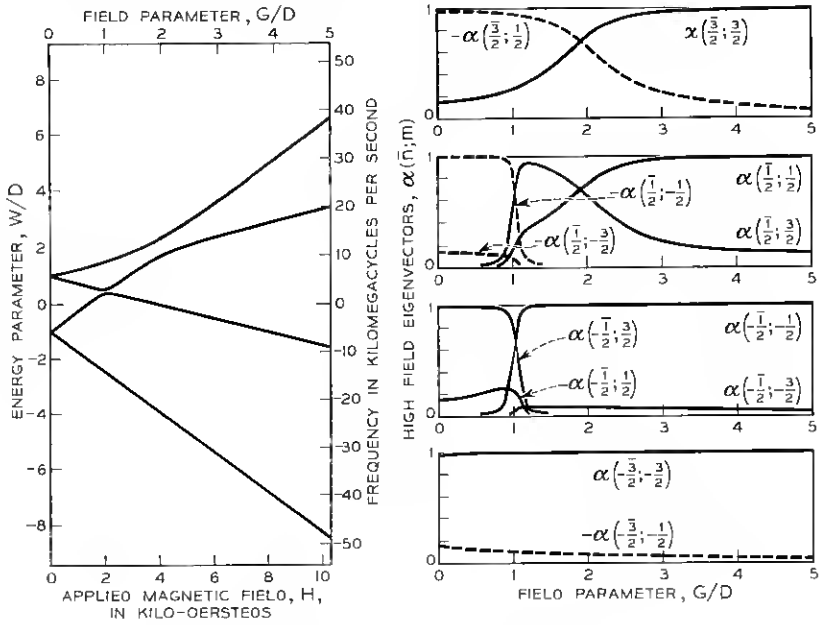

Fig. 2 — Energy levels and eigenvectors at 10°.

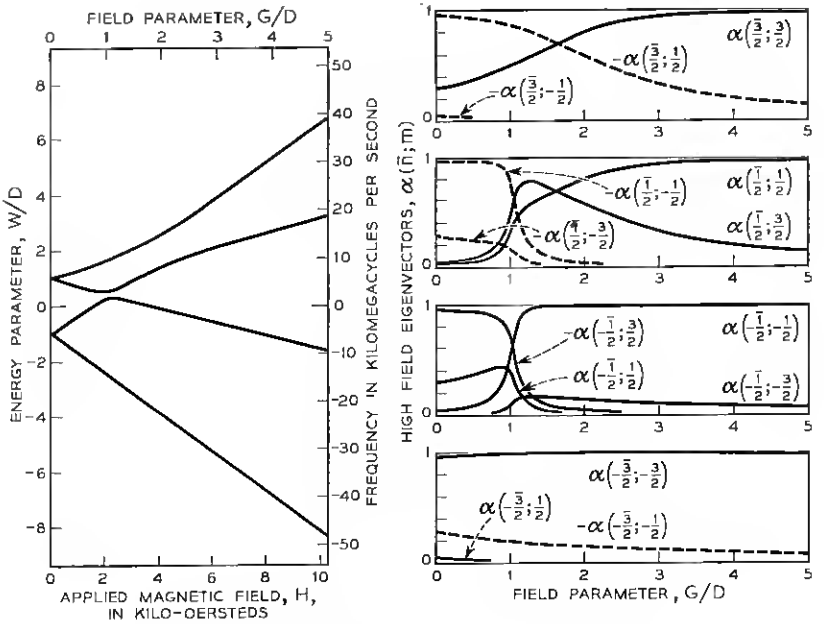

Fig. 3 — Energy levels and eigenvectors at 20°.

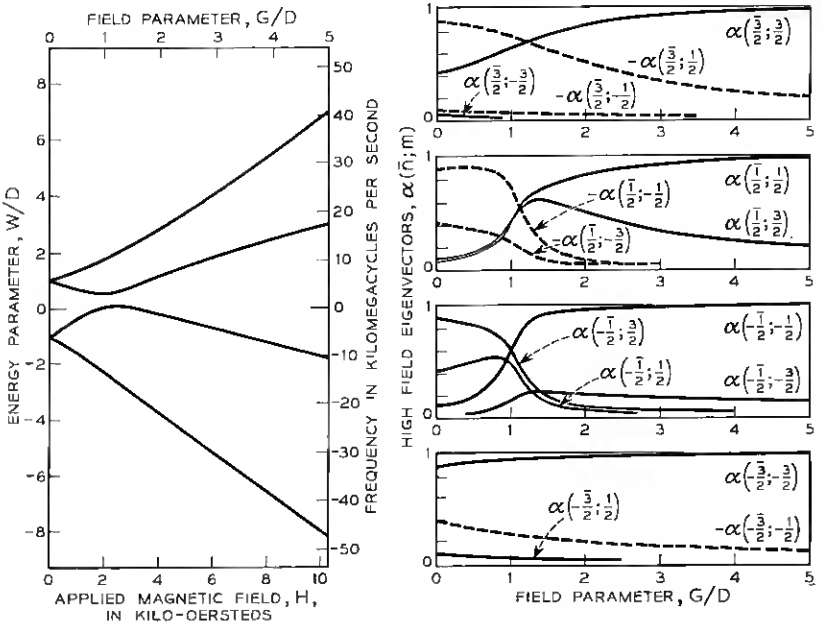

Fig. 4 — Energy levels and eigenvectors at 30°.

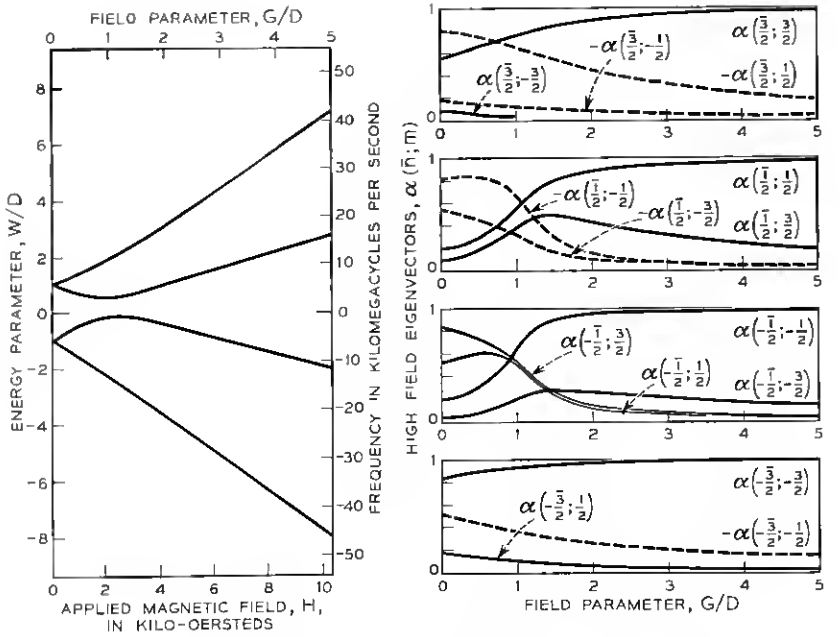

Fig. 5 — Energy levels and eigenvectors at 40°.

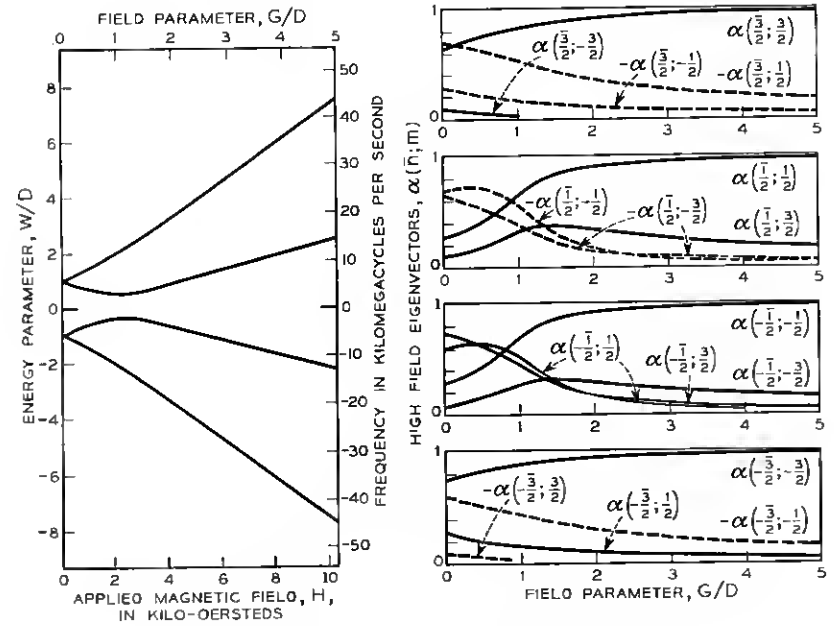

Fig. 6 — Energy levels and eigenvectors at 50°.

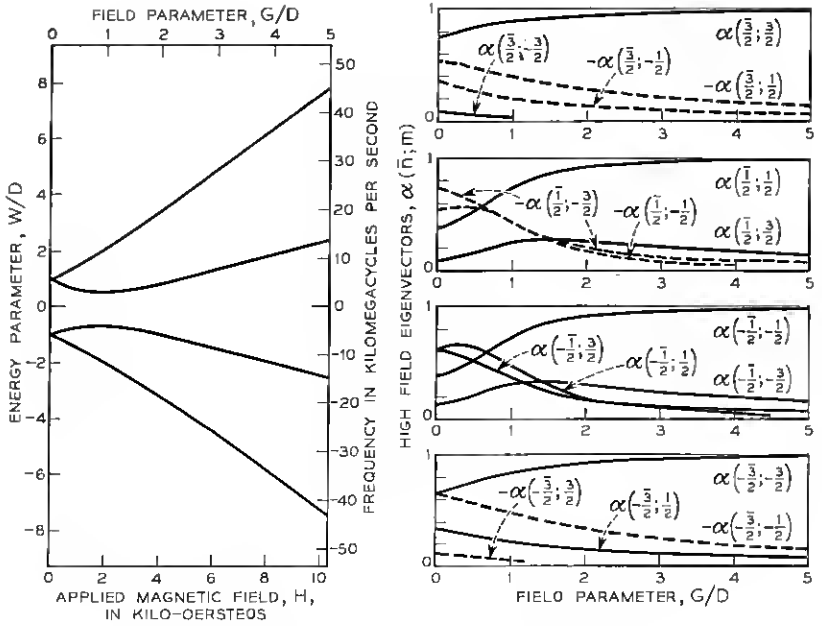

Fig. 7 — Energy levels and eigenvectors at 54.7°.

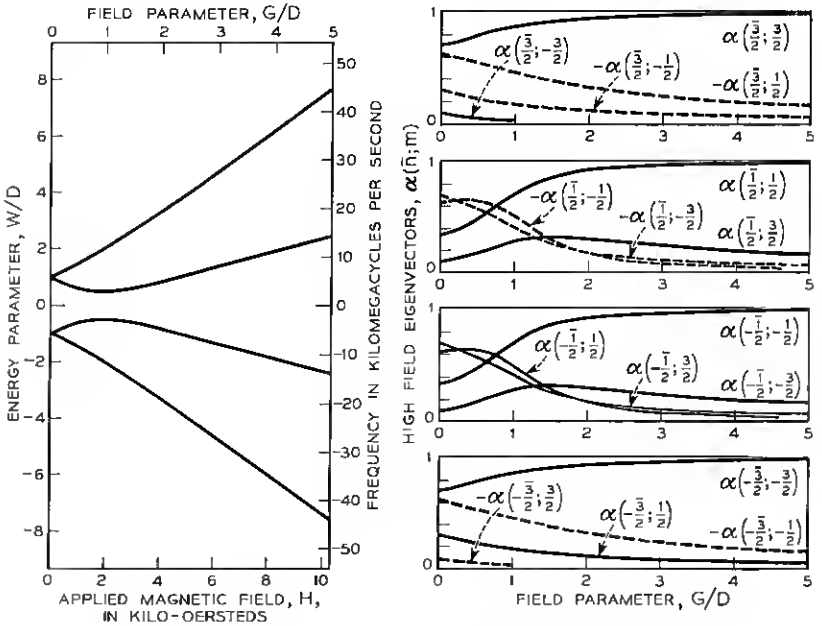

Fig. 8 — Energy levels and eigenvectors at 60°.

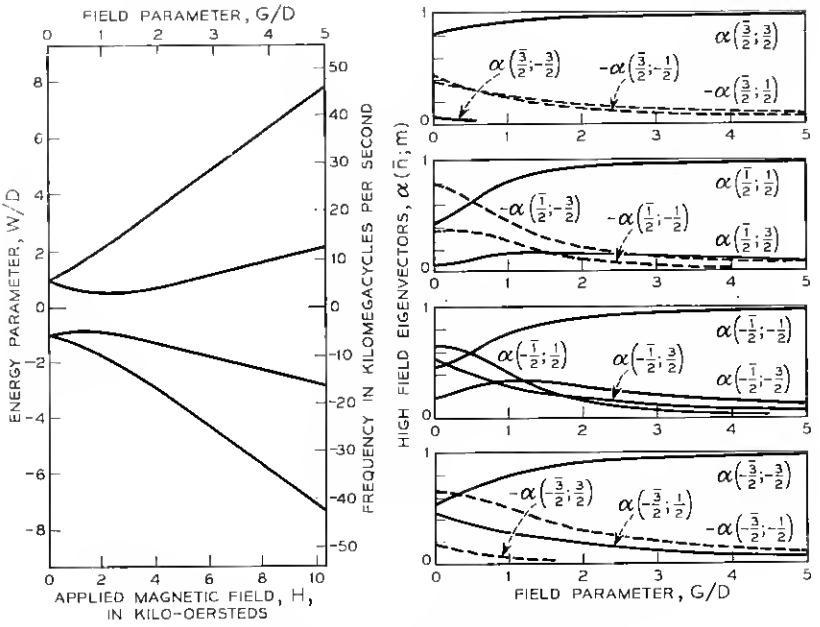

Fig. 9 — Energy levels and eigenvectors at 70°.

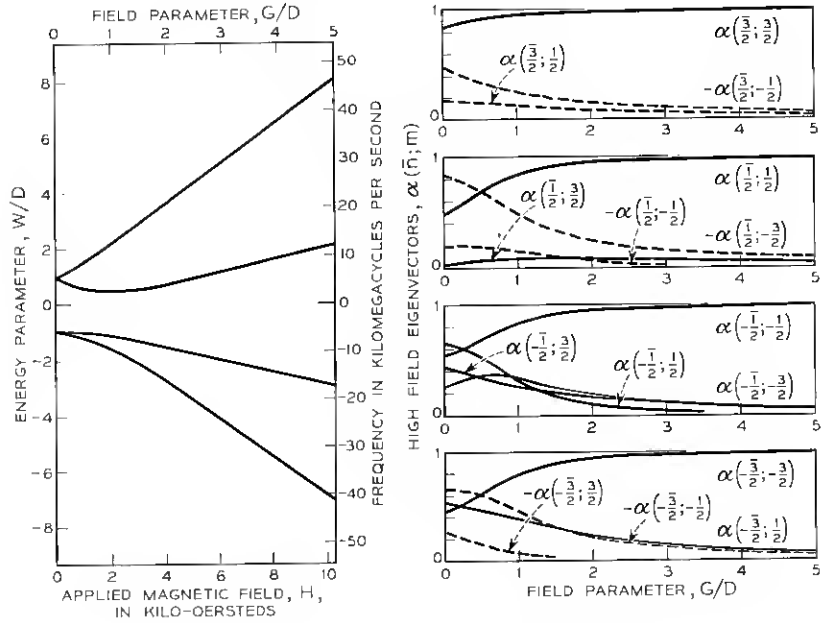

Fig. 10 — Energy levels and eigenvectors at 80°.

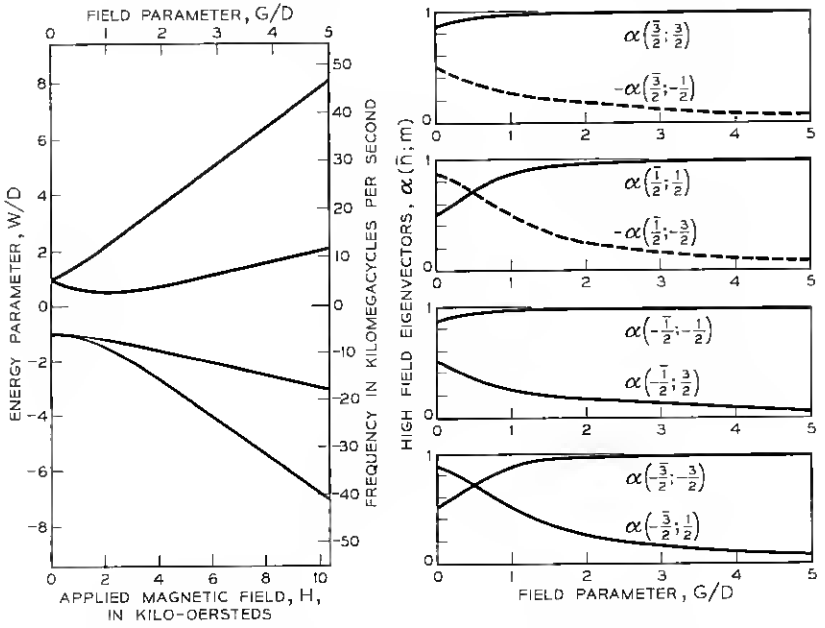

Fig. 11 — Energy levels and eigenvectors at 90°.

This dimensionless representation facilitates computations and reveals more clearly symmetries and singular relations in the energy level scheme. It also permits the use of the same diagrams for ions having the same Hamiltonian but different zero field splitting $2D$. Similar energy level diagrams were computed by P. M. Parker[11] for the case of nuclear spin resonance with nuclear quadrupole splitting present which is described by the same type of Hamiltonian.

As a convenient way to identify the energy levels W, a quantum number $\bar{n}$ ranging from $-\frac{3}{2}$ to $+\frac{3}{2}$ is used *in order of increasing energy*. Thus $W(-\frac{3}{2})$ is the lowest, $W(\frac{3}{2})$ the highest energy level. It is easily shown that, for all angles θ and $x = 0$, $y(-\frac{3}{2}) = y(-\frac{1}{2}) = -1$ and $y(\frac{1}{2}) = y(\frac{3}{2}) = 1$. As a matter of mathematical curiosity, it may be mentioned that, irrespective of θ at $x = 1$, $y(\frac{1}{2}) = 1/2$.

The eigenstates $|\bar{n}\rangle$ (using Dirac's "ket" notation) associated with energy levels $W(\bar{n})$ can be expanded in the form

$$|\bar{n}\rangle = \sum_{m=-3/2}^{3/2} \alpha(\bar{n}; m) \, |m\rangle. \tag{5}$$

Here, $|m\rangle$ are eigenstates of a Zeeman Hamiltonian $\mathcal{H} = g\beta H S_z$. The $\alpha(\bar{n}; m)$ are amplitudes of eigenvector components or, more briefly,

eigenvectors and form a normalized and orthogonal system of coefficients. With high applied magnetic field H, $|\bar{n}\rangle \rightarrow |n\rangle$ and $\alpha(\bar{n}; n) \rightarrow 1$; therefore, $|m\rangle$ are termed high-field eigenstates and $\alpha(\bar{n}; m)$ high-field eigenvectors.

Eigenvectors $\alpha(\bar{n}; m)$ are obtained as solutions of linear homogeneous equation systems, the matrix of which forms the secular equation (4) with the particular eigenvalue $W(\bar{n})$ inserted. Since this matrix depends on φ, the $\alpha(\bar{n}; m)$ are also functions of φ. The computations were carried out for $\varphi = 0$, with θ restricted to $0 < \theta < \pi/2$ and negative sign of $D = -D'$.

This choice implies that the crystalline axis lies in the positive quadrant of the x-z plane and it results in real eigenvectors $\alpha(\bar{n}; m)$. These are plotted in the right-hand sections of Figs. 1 through 11, adjacent to plots of the corresponding eigenvalues $W(\bar{n})$. Negative $\alpha(\bar{n}; m)$ are indicated by dashed lines.

A nonzero φ would, in general, result in new complex eigenvectors $\alpha'(\bar{n}; m) = [\exp i(m - \bar{n})\varphi]\alpha(\bar{n}; m)$. Taking $\pi/2 < \theta < \pi$ or $\varphi = \pi$ would change the sign of every second eigenvector, that is, of those with $m = n \pm 1$ and $m = n \pm 3$. The same is true for a change of sign of D, but then, in addition, every $\bar{n}$ and m and energy eigenvalue has to be replaced by its negative. It is obvious that such transformations do not change the physical situation as far as transition probabilities are concerned.

IV. TRANSITION PROBABILITIES

There are several ways in which transition probabilities could be evaluated and plotted. One way would be to consider transitions induced by radiation of given polarization. With eigenvectors belonging to the Hamiltonian (3), the obvious RF magnetic field polarizations to consider are those with RF H-field linear and parallel to, or circular and perpendicular to, the applied field. But transitions due to any other polarization could be evaluated as well. Perhaps more natural from a theoretical point of view would be an evaluation of the maximum transition probability. This requires a particular—in general—elliptical, polarization for excitation, which of course should be evaluated, too. All polarizations orthogonal to this (which in general are elliptical as well), and which describe a plane in space having complex components, are associated with zero transition probability. Taking into account these different viewpoints and the six transitions which are possible between four energy levels, it appears that an unrealistically high number of graphs would be necessary to describe the transition probabilities properly.

Furthermore, in maser design it is usually sufficient to know the order of magnitude of transition probabilities of particular lines, because often other factors may be more important. Therefore, no plots of transition probabilities are presented. On the other hand, enough of the pertinent formalism is given below so that any transition probability can be evaluated from the eigenvectors plotted.

Following essentially Bloembergen, Purcell and Pound,[12] with slight generalization, the transition probability w describing the rate of transitions per ion from a lower state $\bar{n}$ to a higher state $\bar{n}' > \bar{n}$ is given by

$$w_{\bar{n}\to\bar{n}'} = \frac{1}{4}\left(\frac{2\pi g\beta H_1}{h}\right)^2 g(\nu - \nu_0) \mid \langle \bar{n}' \mid S_1 \mid \bar{n} \rangle \mid^2. \tag{6}$$

Here H_1 is the amplitude of the exciting RF magnetic field, $g(\nu - \nu_0)$ is a normalized function describing the line shape $\int g(\nu - \nu_0)\, d\nu = 1$, and S_1 is a spin operator reflecting the polarization of the inducing RF magnetic field. If the RF magnetic field is described by the real parts of $H_x = H_1 a e^{i\omega t}$, $H_y = H_1 b e^{i\omega t}$, $H_z = H_1 c e^{i\omega t}$ with "complex direction cosines" a, b, c accounting for elliptical polarization,

$$a^*a + b^*b + c^*c = 1,$$

then

$$S_1 = a^*S_x + b^*S_y + c^*S_z\,. \tag{7}$$

Matrix elements for S_1 occurring squared in (6) are linear combinations of the following three:

$$\langle \bar{n}' \mid S_z \mid \bar{n} \rangle = \sum_{m=-3/2}^{+3/2} m\alpha(\bar{n}'; m)\alpha(\bar{n}; m), \tag{8}$$

$$\langle \bar{n}' \mid S_+ \mid \bar{n} \rangle = \sum_{m=-3/2}^{+1/2} [S(S+1) - (m+1)m]^{1/2}\alpha(\bar{n}'; m+1)\alpha(\bar{n}; m), \tag{9}$$

$$\langle \bar{n}' \mid S_- \mid \bar{n} \rangle = \sum_{m=-1/2}^{+3/2} [S(S+1) - (m-1)m]^{1/2}\alpha(\bar{n}'; m-1)\alpha(\bar{n}; m). \tag{10}$$

The square root in (9) and (10) takes on the values $\sqrt{3}$, 2 and $\sqrt{3}$. For example, with linear polarization in the z-direction, $H_z = H_1 \cos \omega t$ and $S_1 = S_z$. For circular polarization perpendicular to the z-direction,

$H_x = (1/\sqrt{2})H_1 \cos \omega t$, $H_y = \pm(1/\sqrt{2})H_1 \sin \omega t$ and $S_1 = (1/\sqrt{2})S_\pm$. For linear polarization in the x direction, $H_x = H_1 \cos \omega t$ and $S_1 = S_x = \frac{1}{2}(S_+ + S_-)$. Similarly, in the y direction $H_y = H_1 \cos \omega t$ and $S_1 = S_y = (1/2i)(S_+ + S_-)$.

The expression (7), or more correctly, the associated matrix element, can be interpreted as a scalar product of (a^*, b^*, c^*) with $\langle \bar{n}' \mid S \mid \bar{n} \rangle$. It should be noted that, in general, all components can be complex. As a consequence of this interpretation, the maximum transition probability occurs if H_{rf} or (a, b, c) is parallel in space and conjugate complex in phase to $\langle \bar{n}' \mid S \mid \bar{n} \rangle$. Since for real eigenvectors the matrices (8), (9), (10) are all real, it follows that $\langle \bar{n}' \mid S_x \mid \bar{n} \rangle$ and $\langle \bar{n}' \mid S_z \mid \bar{n} \rangle$ are real, whereas $\langle \bar{n}' \mid S_y \mid \bar{n} \rangle$ is imaginary. Thus, for all ruby lines, the polarization for maximum transition probability will be a linear combination of H_x and H_z components with an H_y component in quadrature. In a similar fashion, a set of complex direction cosines can be found which causes the scalar product of (a^*, b^*, c^*) with $\langle \bar{n}' \mid S \mid \bar{n} \rangle$, and hence the transition probability, to vanish. These vectors (a, b, c) describe a plane orthogonal to the vector for maximum transition probability.

It should be noted that frequently the complete formula (6) is not used to evaluate and compare transition probabilities. Instead, usually only the squared matrix element $| \langle \bar{n}' \mid S_1 \mid \bar{n} \rangle |^2$ is computed and this is then compared with a simple standard transition. The obvious standard is the transition $-1/2 \rightarrow +1/2$ of an $S = 1/2$ Zeeman doublet induced by circular polarization. This is described, in our notation, by $| \langle +1/2 \mid (1/\sqrt{2})S_+ \mid -1/2 \rangle |^2 = 1/2$. Accordingly, transitions involving a squared matrix element of order 1 or greater are considered strong, while perhaps 1/100 is typical of weak transitions.

V. SPECIAL CASES

5.1. $\theta = 0°$.

The energy levels are parts of straight lines $y = 1 \pm \frac{1}{2}x$, $-1 \pm \frac{3}{2}x$ with change of slope for some of them at $x = 1$ and 2. Eigenvectors are ± 1 and 0 only, again joined for some levels at $x = 1$ and 2. The minus sign of eigenvectors at 0° has no significance; it is only used to preserve continuity to neighboring angles.

At $\theta = 0°$ and $x < 2$, the labeling of energy levels by high field quantum numbers *in order of increasing energy* is perhaps not the usual one. In this paper, however, it seems appropriate because, with this terminology, in going from $\theta = 0°$ to other orientations, the notation of states

stays the same. It may be pointed out that energy levels defined in this fashion should be considered as continuous functions of applied field without cross-overs (see Fig. 1). The reason is that any off-diagonal perturbation will indeed prevent levels from intercepting by perturbation theory arguments.

Only three transitions are allowed:

$$0 < x < 1: \langle +\tfrac{3}{2} \mid S_+ \mid +\tfrac{1}{2}\rangle^2 = 4$$

$$\langle +\tfrac{3}{2} \mid S_- \mid -\tfrac{1}{2}\rangle^2 = \langle +\tfrac{1}{2} \mid S_+ \mid -\tfrac{3}{2}\rangle^2 = 3,$$

$$1 < x < 2: \langle +\tfrac{3}{2} \mid S_+ \mid -\tfrac{1}{2}\rangle^2 = 4$$

$$\langle +\tfrac{3}{2} \mid S_- \mid +\tfrac{1}{2}\rangle^2 = \langle +\tfrac{1}{2} \mid S_+ \mid -\tfrac{3}{2}\rangle^2 = 3,$$

$$2 < x: \quad \langle +\tfrac{1}{2} \mid S_+ \mid -\tfrac{1}{2}\rangle^2 = 4$$

$$\langle +\tfrac{3}{2} \mid S_+ \mid +\tfrac{1}{2}\rangle^2 = \langle -\tfrac{1}{2} \mid S_+ \mid -\tfrac{3}{2}\rangle^2 = 3.$$

It is interesting to note that, for $0 < x < 2$, one transition requires opposite polarization from the others. This was verified in an experiment. Resonance absorption was measured for this and another transition in a propagating comb-type slow-wave structure having regions of predominantly circular polarization. Reversal of applied magnetic field results in drastic increase of one and reduction of the other line.

5.2. $\theta = 54.74°$, $\cos^2\theta = 1/3$.

For this angle, the fourth-order secular equation reduces to a biquadratic one. The four eigenvalues are $y = \pm[1 + \frac{5}{4}x^2 \pm (3x^2 + x^4)^{1/2}]^{1/2}$. This implies an up-down symmetry $y(-\vec{n}) = -y(\vec{n})$. The closest approach of the two middle eigenvalues is $y(+\frac{1}{2}) - y(-\frac{1}{2}) = 1$ at $x = 1$. A similar symmetry relation holds for eigenvectors $\alpha(-\vec{n}; -m) = (\vec{n}m/|\,\vec{n}m\,|)\alpha(\vec{n}; m)$. As a consequence, some transition probabilities for linear polarization are identical, namely

$$\langle -\tfrac{1}{2} \mid S_z \mid -\tfrac{3}{2}\rangle = \langle +\tfrac{3}{2} \mid S_z \mid +\tfrac{1}{2}\rangle$$

and

$$\langle +\tfrac{1}{2} \mid S_z \mid -\tfrac{3}{2}\rangle = -\langle +\tfrac{3}{2} \mid S_z \mid -\tfrac{1}{2}\rangle.$$

The analogous is not true for other polarizations.

5.3. $\theta = 90°$.

The secular equation can be factorized into two quadratic equations with the solutions

$$y(\tfrac{3}{2}) = \frac{x}{2} + (1 + x + x^2)^{1/2},$$

$$y(\tfrac{1}{2}) = -\frac{x}{2} + (1 - x + x^2)^{1/2},$$

$$y(-\tfrac{1}{2}) = \frac{x}{2} - (1 + x + x^2)^{1/2},$$

$$y(-\tfrac{3}{2}) = -\frac{x}{2} - (1 - x + x^2)^{1/2}.$$

Each state contains only two eigenvectors, namely $\alpha(\bar{n};\ n)$ and $\alpha(\bar{n};\ n \pm 2)$. In addition, $\alpha(\bar{n};\ n) = \alpha(\overline{n \pm 2};\bar{n} \pm 2)$ and $\alpha(\bar{n};\ n \pm 2) = -\alpha(\overline{n \pm 2};\ n)$. As a result, transition probabilities between adjacent

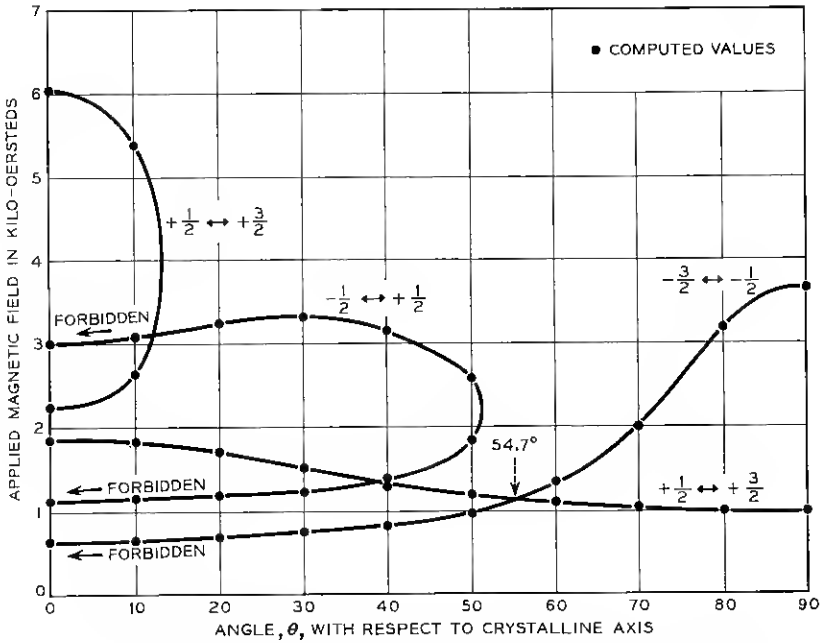

Fig. 12 — Paramagnetic resonance spectrum of Cr^{+++} ions in ruby at signal frequency 5.18 kmc.

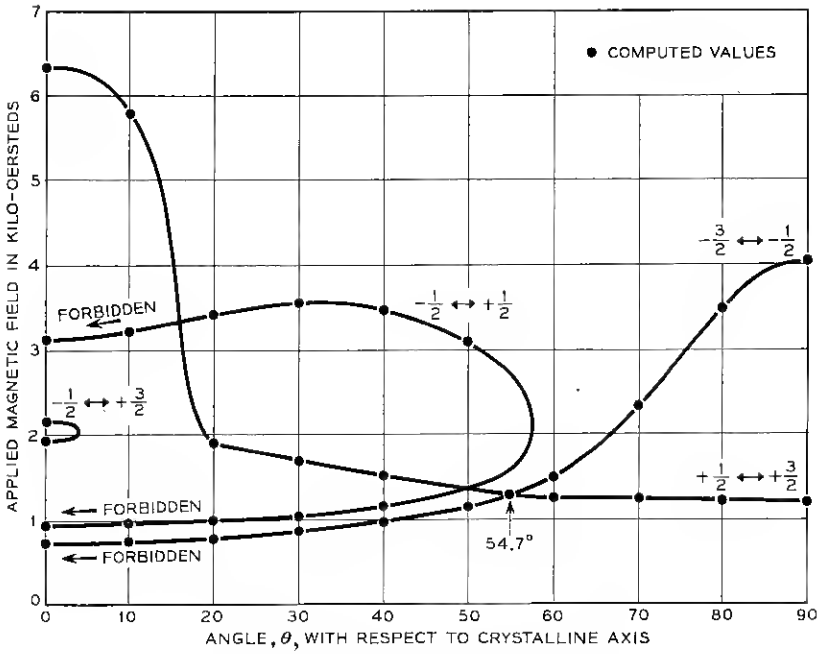

Fig. 13 — Resonance spectrum at 6.08 kmc.

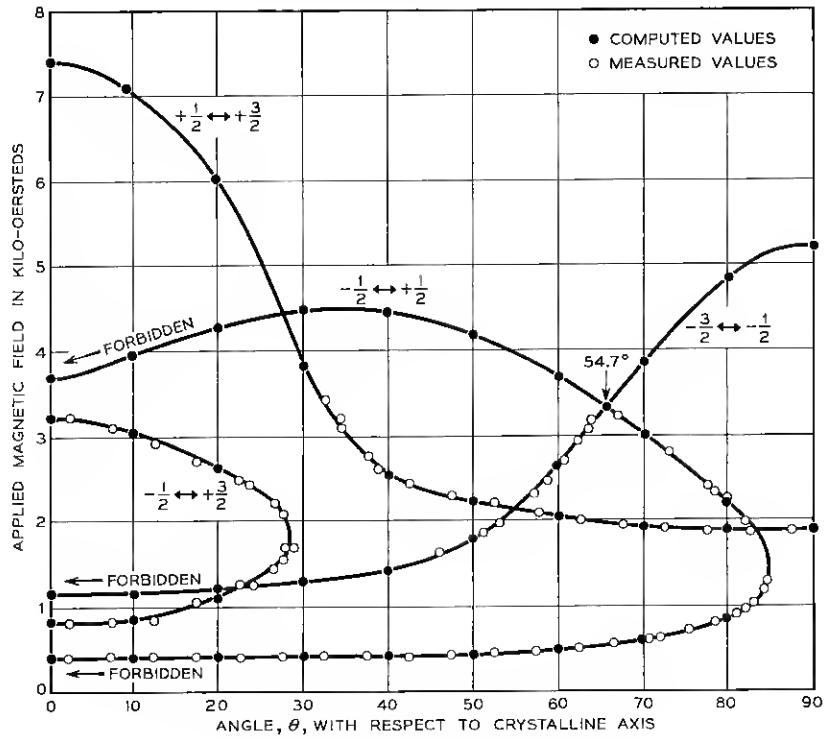

Fig. 14 — Resonance spectrum at 9.30 kmc.

levels $\bar{n} \rightarrow \overline{n+1}$ contain only matrix elements of S_+ and S_-, the same being true for $-\frac{3}{2} \rightarrow +\frac{3}{2}$. Double jumps $\bar{n} \rightarrow \overline{n+2}$ are described by nonvanishing elements of S_z only.

VI. PARAMAGNETIC RESONANCE SPECTRA

In Figs. 12 through 17 some resonance spectra are shown for signal frequencies of 5.18, 6.08, 9.30, 12.33, 18.2 and 23.9 kmc. The plots show resonance fields as functions of the angle between crystalline axis and applied field. Measurements have been carried out at all of these frequencies to varying extents, although measured values are recorded only on Figs. 14 and 15. Generally, these spectra have been used in the laboratory to align ruby crystals by resonance for maser experiments. They have proved accurate to about ±50 gauss.

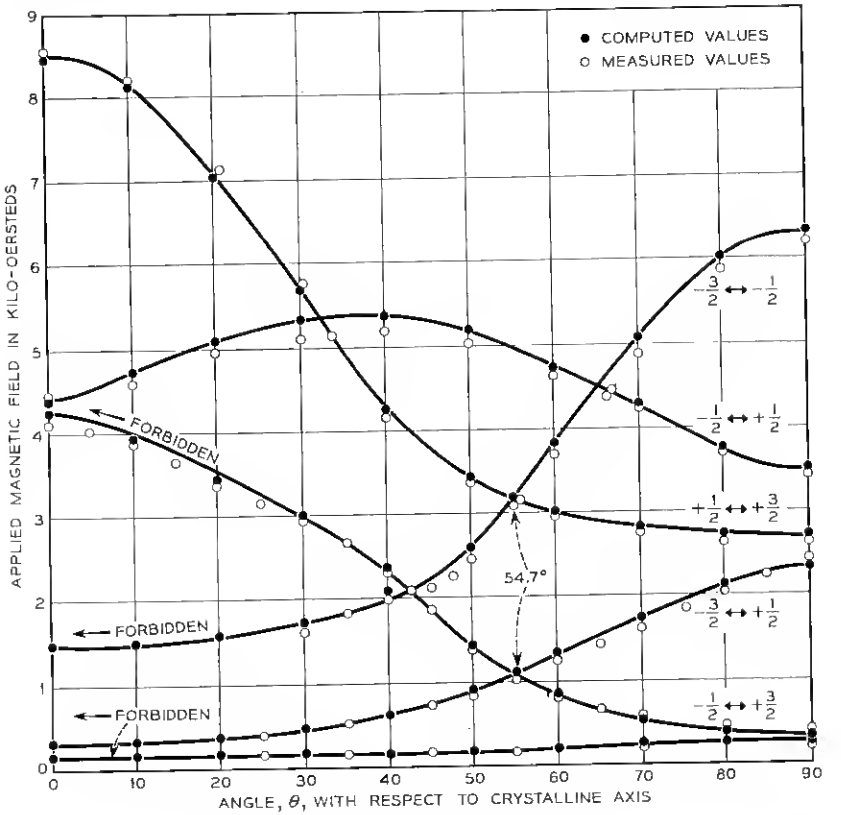

Fig. 15 — Resonance spectrum at 12.33 kmc.

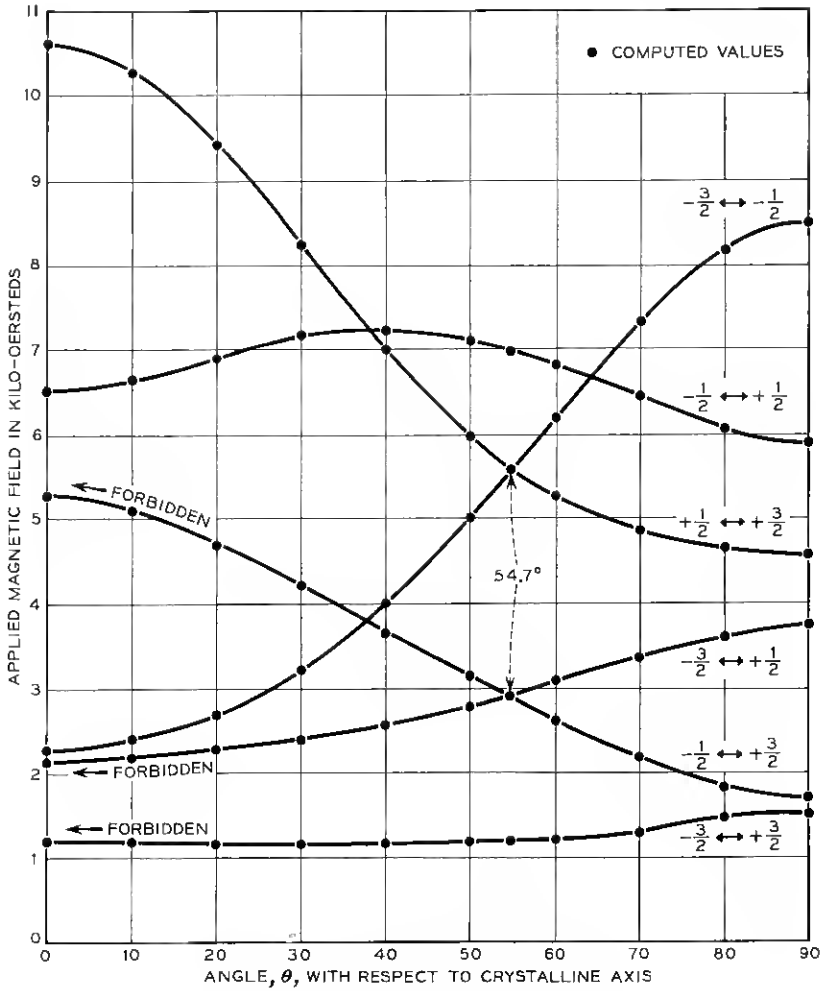

Fig. 16 — Resonance spectrum at 18.2 kmc.

Measurements at 9.3 kmc are an extension of Geusic's work[4] and confirm his results. Results at 12.33 kmc show some discrepancy between theory and experiment, which, however, is believed to be caused by inadequate magnetic field measuring equipment used in an experiment designed for other purposes. As a general rule, the spectra show two looping lines if $\nu < 2D$. Lines marked "forbidden" are strictly forbidden at 0° only. Usually, however, they can be followed quite close to 0° by

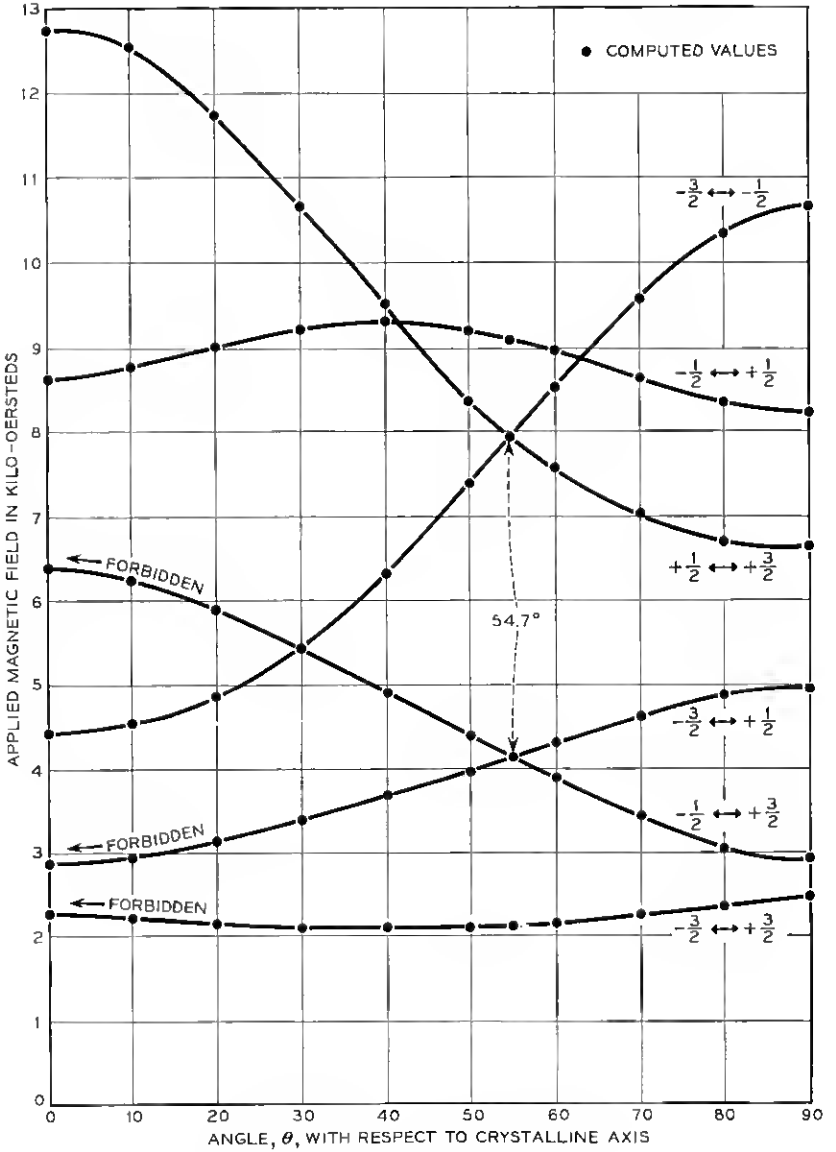

Fig. 17 — Resonance spectrum at 23.9 kmc.

use of more sensitivity in the spectrometer. An exception is the line shown on the graphs having the lowest resonance field at 0° if $\nu < \frac{6}{5}D'$. It has the second lowest resonance field if $\frac{6}{5}D' < \nu < \frac{3}{2}D'$ and the third lowest if $\frac{3}{2}D' < \nu < 3D'$. It originates between $-\frac{3}{2}$ and $+\frac{3}{2}$ eigenstates at 0° and is more strongly forbidden than the other forbidden lines; hence it usually ceases to be measurable at about 30°.

For reasons of symmetry, all lines approach 0° and 90° with zero slope $dH/d\theta$. Experimentally, it has been found that most lines are rather narrow at 90° and similarly at 0°, whereas they broaden in proportion with $dH/d\theta$. This behavior is expected from crystalline imperfections if these can be interpreted as fluctuations throughout the crystal of the direction of the crystalline axis.

VII. ACKNOWLEDGMENT

The author wishes to thank many colleagues at Bell Telephone Laboratories for suggestions in the course of this study. He is particularly indebted to H. E. D. Scovil and J. E. Geusic. Miss M. C. Gray programmed and supervised the numerical calculations.

REFERENCES

1. Bloembergen, N., Proposal for a New-Type Solid-State Maser, Phys. Rev., **104**, October 15, 1956, p. 324.
2. Scovil, H. E. D., Feher, G. and Seidel, H., Operation of a Solid-State Maser, Phys. Rev., **105**, January 15, 1957 p. 762.
3. Scovil, H. E. D., The Three-Level Solid-State Maser, Trans. I.R.E., **MTT-6**, January 1958, p. 29.
4. Makhov, G., Kikuchi, C., Lambe, J. and Terhune, R. W., Maser Action in Ruby, Phys. Rev., **109**, February 15, 1958, p. 1399.
5. Bleaney, B. and Stevens, K. W. H., Paramagnetic Resonance, Rep. Prog. Phys., **16**, 1953, p. 107.
6. Bowers, K. D. and Owen, J., Paramagnetic Resonance II, Rep. Prog. Phys., **18**, 1955, p. 304.
7. Manenkov, A. A. and Prokhorov, A. M., J. Exp. Theor. Phys. (U.S.S.R.), **28**, 1955, p. 762.
8. Geusic, J. E., Phys. Rev., **102**, June 15, 1956, p. 1252; also Ph.D. dissertation, Ohio State Univ., 1958.
9. Zaripov, M. and Shamonin, I., J. Exp. Theor. Phys. (U.S.S.R.), **30**, 1956, p. 291.
10. Bruger, K., Ph.D. dissertation, Ohio State Univ., 1958.
11. Parker, P. M., J. Chem. Phys., **24**, 1956, p. 1096.
12. Bloembergen, N., Purcell, E. M. and Pound, R. V., Relaxation Effects in Nuclear Magnetic Resonance Absorption, Phys. Rev., **73**, April 1, 1948, p. 679.